MAGNETIC SPIN RESONANCE

1. Introduction

Magnetic spin resonance techniques are among the most powerful methods available for determining primary structure, conformation, and local dynamic properties of molecules in liquid, solid, and even gas phases of organic and inorganic molecules. These methods measure the interactions between matter and external radio frequency (rf) fields in the presence of a static external magnetic field. Under suitable conditions the measurements also may be sufficiently quantitative for analytical applications. Although much of the theory is similar, spin resonance experiments are subdivided into nuclear magnetic (nmr) and electron spin (esr) resonance methods. The first of these techniques has led to a newer field of study, magnetic resonance imaging, covered elsewhere (see MEDICAL IMAGING TECHNOLOGY). Nuclear magnetic resonance originally was carried out in continuous wave (CW) mode where the external magnetic field was systematically varied to match the resonance conditions for individual nuclei. As of this writing almost all experiments are done using the pulse or Fourier transform (ft) mode of operation and that mode is discussed herein. The reader is encouraged to consult the references for more detailed information in specific areas. References, selected for both utility and clarity, may not be the original citation of primary work. Several excellent textbooks for both nmr (1,2) and esr (3) exist.

2. Theoretical Background

An unpaired electron or an atomic nucleus, unless it has even integral values for both atomic mass and atomic number, has a nonzero angular momentum and measurable magnetic moment. Both the electron and the hydrogen nucleus or proton, ^{1}H, have a spin, I, of $1/2$. Other nuclei may have larger values of I (see Table 1). A given nucleus can exist in any of $2nI + 1$ states described by a nuclear spin quantum number, m_i, ranging from $+I$ (lowest energy) to $-I$ (highest energy) in unit steps. When placed in an external static magnetic field, B_0, the difference in energy, ΔE, between adjacent states is given by:

$$\Delta E = h\omega_0/2\pi = h\gamma B_0/2\pi = h\nu$$

where h is Planck's constant (6.626×10^{-34}J·s), γ is the magnetogyric ratio, and $\omega_0/2\pi = \nu$ is the Larmor frequency in Hertz. The value of γ for an electron is about 660 times larger than for a hydrogen atom. As shown in Figure 1 for the spin $1/2$ case, the precise value of both the energy and Larmor frequency is proportional to the strength of the static external field. The relative population, $N\beta/N\alpha$, of the two energy levels is described by the Boltzmann relation,

$$N_\beta/N_\alpha = \exp(-\Delta E/kT)$$

leadingto population differences on the order of 5 parts in 10^5 for ^{1}H at 300 K and 7.05 T (70.5 kG) (70.5kG) = B_0.

2.1. Nuclear Magnetic Resonance. The interaction of a nucleus with B_0 is usually described using vector notation and models as in Figure 2 where the bulk magnetization, M, and the static field B_0 are initially parallel to z. A radio frequency pulse is applied in the xy plane for a duration of t μs, tipping the magnetization by θ radians where $\theta = \gamma B_1 t$. The duration of the 90° pulse required to completely shift magnetization into the xy plane is thus inversely proportional to B_1. The change in orientation of individual spins with respect to the external field is referred to as resonance. Because the net magnetization is now inclined with respect to B_0 in response to the rf source, it precesses about the z axis at the Larmor frequency. The concept of a rotating frame, in which a new set of axes, x' and y', rotate about z at the same frequency as the precessing nucleus, ie, γB_0, is conceptually convenient. Because the rotating frame is the standard reference system for describing magnetic resonance experiments, the prime designations for that system usually are omitted in most theoretical discussions. The application of an rf field, B_1, is considered to be along x' and this leads to a tipping of the magnetization vector in the $y'z'$ plane, as shown in Figure 2. The magnitude of the tipping is determined by the pulse width or duration, ie, the length of time, typically in μs, that B_1 is applied. For a $\pi/2$ or 90° pulse the magnetization is rotated completely into the $x'y'$ plane with no remaining component along z. This is equivalent to equalizing the population of the spin states. Continuation of the irradiation results in a continuing rotation of the magnetization about the x'-axis. It is possible to create π, $3\pi/2$, or any other pulse width by varying the duration of the irradiation. It is also possible to saturate a spin simply by continuing to irradiate with rf of the correct frequency. While a spin is saturated, it provides no resonance signal. When the rf is switched off, the system attempts to reestablish its equilibrium distribution of spins. Whereas 90° or $\pi/2$ pulses provide the maximum possible signal from a single pulse, shorter pulses are used in many cases when the rate of restoring magnetic equilibrium is slow.

The precessing magnetization induces a current in the detector coil which surrounds the sample and is centered on the laboratory y-axis. The time dependent fluctuation in this current decays in intensity as the spin distribution returns to its equilibrium distribution. The response to a single pulse is referred to as a free induction decay (FID) or transient and is converted to a digital form by an analogue-to-digital converter (ADC) for storage in a computer file. A principal advantage of the pulse nmr spectrometer over CW methods lies in the fact that the pulse experiment can be repeated after a suitable delay with the FID from each pulse train added to the accumulating time domain spectrum. The observed signal is a composite of a true signal from the experiment and a noise component. However, the increase in magnitude of the true signal is proportional to the number of transients which are acquired, whereas the noise increases with the square root of the number of transients. This additivity in the time domain permits experiments utilizing nuclei such as ^{13}C which have low natural abundance, ie, isotopically dilute spin systems.

In ft/nmr the detected signal is the sum of the individual decays for all of the nuclei. To convert this information back into a frequency-dependent form in which spectra are generally viewed, it is necessary to apply a Fourier

transformation. Mathematically this is expressed as

$$f(\omega) = \int f(t)\exp(i\omega t)dt$$

where $f(\omega)$ is the frequency domain spectrum and $f(t)$ is the time-dependent fluctuation of the amplitude in the composite nmr signal. Because $f(t)$ is real, $f(\omega)$ has both real, absorption spectrum, and imaginary, dispersion mode components. When computing this transformation, the absolute value of the phase angle is initially unknown but can be determined from the boundary conditions. The best value for this angle makes each peak in the real component symmetric about its center and always positive. The Cooley-Tukey fast Fourier algorithm permits computation of the transformation for several thousand data points in about 1 s, which is essential to this and other ft methods (4) (see also CHEMOMETRICS).

The time constants associated with the restoration of magnetic equilibrium after application of a pulse are referred to as relaxation times and their reciprocals as relaxation rates. Relaxation may occur by any of several different mechanisms involving either longitudinal, T_1, or transverse, T_2, processes. Historically, the terms spin–lattice and spin–spin were used to refer to T_1 and T_2 relaxation times, respectively. The first of these involves the restoration of magnetization to the z direction and controls the rate at which the experiment can be repeated. The value of T_2 is determined by all processes contributing to loss of magnetization in the xy plane. For small, freely tumbling molecules in solution, the values of these two constants are often nearly equal and range from a few hundred ms to s in duration. For large molecules, eg, synthetic polymers, proteins (qv), and nucleic acids (qv), local magnetic field fluctuations establish very short T_2 values in both liquid and, especially, solid phases. Molecular scale rigidity, especially in crystalline systems, also results in significantly longer T_1 values which may exceed 100 s.

Because the energy differences between adjacent levels are very small in magnetic resonance experiments, the transition probabilities are also very small in the absence of local field fluctuations. Dipole–dipole interactions are the dominant mechanism for creating local field fluctuations and these decrease in intensity with the sixth power of the internuclear distance, so that only the closest nuclei have an appreciable effect on the relaxation rate for a given atom. The strength of the interaction also depends on the square of the product of the gyromagnetic ratios of the interacting nuclei. Other mechanisms, such as quadrupolar relaxation, may become important if either of the interacting nuclei is paramagnetic or the quadrupolar moment (see Table 1) is significant.

At a minimum, knowledge of relaxation times is important in determining the rate at which the pulse experiment can be repeated and successive transients added to the FID. The delay between acquisitions may be tuned for either minimum acquisition time, ie, short delays, or for uniform sensitivity by setting the delay to at least five times the longest T_1 in the system. Relaxation behavior can also be related to molecular structure and organization, although the process is less straightforward than for integrations, spin–spin couplings, or chemical shifts. The values of both T_1 and T_2 are dependent on the magnitude of the external field B_0. The relative values of T_1 and T_2 are also strongly influenced by the

rate of molecular tumbling, which is usually measured as $(\tau_c)^{-1}$ where τ_c is the rotational correlation time. In the short τ_c regime ($<10^{-10}$ s at 400 MHz for ^{1}H) T_1 and T_2 are nearly equal; in the long, ie, slowly tumbling nuclei ($\tau_c > 10^{-9}$s), regime T_1 increases and T_2 decreases exponentially with increasing τ_c.

One additional phenomenon which plays an increasingly important role in nmr-based structure determination is the nuclear Overhauser effect (NOE) (5). The NOE originates in relaxations arising from dipole–dipole interactions through space and decreases in intensity with r^6_{IS}, where r_{IS} is the internuclear separation of two mutually relaxing spins. In organic molecules, this means that the effect is dominated by individual protons and their interaction with nearby nuclei in the same molecule. The effect is not evident in coupled ^{13}C or ^{1}H spectra, but can alter intensities in ^{1}H decoupled ^{13}C spectra causing enhancements of some peaks by up to a 200%. Inverse gated decoupling experiments where the ^{1}H decoupling is turned on for the acquisition period and off during a preparation period, which is long compared to any of the relaxation times, provides a method for eliminating NOE influences on the decoupled spectrum. The observation of an NOE between two nuclei implies that the nuclei are close together in space, typically separated by less than 0.45 nm. The failure to observe an NOE does not, however, mean that the nuclei are far apart, because the relaxation rate also depends on τ_c.

Resolution is an important consideration in any experiment involving a number of closely spaced maxima. The digital resolution (DR) achievable in an nmr spectrum is defined by the relation

$$\mathrm{DR} = 2\cdot(\text{sweep width})/(\text{number of data points})$$

The acquisition time duringwhich the spectrum is acquired is the reciprocal of DR. In practice this resolution is only achievable if the signal from the sample persists throughout the acquisition time. When molecular motion is slow as in large molecules or viscous solutions, T_2 relaxation is very fast, leading to broad lines in the spectrum, and resolution is limited by the natural line width $1/T^2$. Because the mean instrumental noise amplitude is constant during acquisition, data points acquired at the beginning of the FID have a higher signal-to-noise ratio (SNR) than those at the end of the FID. Window (apodization) functions define the weights assigned to individual data points in the FID and may lead to SNR or resolution enhancement in the frequency spectrum. Multiplication of points in the FID by an exponentially decaying function is referred to as line broadening, whereas a negative exponential sharpens individual peaks. The sine–bell function, which places greatest importance on the middle region of the FID and less on either extreme, and its variations are widely used because of the ability to sharpen the spectrum while minimizing noise effects. It is common practice in nmr data processing to expand, or zero-fill, the FID from 2^N to 2^{N+1} data points before transformation.

If the actual signal has not vanished by the end of the acquisition period then the FID is truncated, producing artifacts in the spectrum. This can be corrected either by increasing the number of data points in the FID or by decreasing the sweep width and concomitantly increasing the acquisition time. The former

method may be restricted by computing power and processing time. Both of these approaches result in increased digital resolution in the processed spectrum.

2.2. Electron Spin Resonance. Electron spin resonance (esr) also known as electron paramagnetic resonance (epr) is a second magnetic resonance technique which finds particular applications in the study of free radicals, paramagnetic species, and other molecules containing an unpaired electron. The electron has a spin of 1/2 and, because of its low mass, a gyromagnetic ratio of 1760 rad/(T·s). Field strengths required for esr are much lower, typically 0.34 T (3.4 kG) and the frequencies higher (9–35 GHz) than for nmr. Data are usually reported in terms of intensity, signal strength, versus energy where the energy for a transition is usually expressed as

$$\Delta E = g\beta H$$

where g is the dimensionless splitting constant equal to 2.0023 for a free electron, β is the Bohr magnetron, μ_B ($\mu = 9.2732 \times 10^{-24}$ J/T), and H is the external field strength. Experimental data are usually reported as first derivative spectra rather than in the absorption mode typical of nmr. Peak positions are defined by the position where the spectrum changes sign. Couplings between the unpaired electron and nearby nuclei create hyperfine interactions with characteristic hyperfine splitting constants, ΔH, expressed in Gauss ($1\text{G} = 10^{-4}\text{T}$). Line shape, as in nmr, is dependent on correlation times. Three τ_c regimes are recognized. The fast, slow, and very slow regions are recognized as $10^{-11} - 10^{-9}$s, $10^{-9} - 10^{-7}$s, and $10^{-7} - 10^{-3}$s, respectively. Because of the very short lifetimes of many organic free radicals and radical ions, measurements are often made at low, ie, liquid nitrogen or liquid helium, temperatures (see CRYOGENICS).

3. Equipment

3.1. Nuclear Magnetic Resonance. In 1994 there were three principal vendors of nmr instrumentation in the U.S., Bruker Instruments (Billerica, Mass.), JEOL USA, Inc. (Peabody, Mass.), and Varian Associates (Palo Alto, Calif.). Details of instrumentation are best obtained directly from manufacturers. A schematic illustrating the principal components of a ft/nmr spectrometer is shown in Figure 3.

Magnets in high field nmr spectrometers are cryostats having niobium alloy wound solenoids, which are superconducting at liquid helium temperatures (4 K) (see MAGNETIC MATERIALS; NIOBIUM AND NIOBIUM COMPOUNDS). Because the wire has no resistance at this temperature, the magnet does not require additional energy to maintain constant current and hence constant field strength. In modern nmr spectrometers the magnetic field strength, B, ranges from 1.4–17.6 T (14–176 kG), corresponding to observation frequencies for ^{1}H of 60–750 MHz. Three critical considerations for these magnets are field strength, field stability (drift), and field homogeneity. The advantages of higher field strength are better sensitivity and resolving power. However, in selecting a new instrument these properties must be balanced against cost. As of this writing (1994) a good rule of thumb for the cost of an nmr spectrometer up to 500 MHz is approximately

$1000/MHz for a basic spectrometer. The 600-MHz and 750-MHz spectrometers typically cost about $1.0 and $2.5 $\times 10^6$, respectively.

Long-term field stability is maintained by the use of a deuterium lock signal. Because deuterated solvents have a constant Larmor frequency at a given field strength, these provide a convenient reference point. The deuterium lock system uses a feedback control loop to monitor the deuterium frequency and make small adjustments in the static field maintaining a constant position for the deuterium signal. To illustrate the importance of minimizing drift in the static field, carbon-13 resonances often have line widths at half height of 0.1 Hz. A static field drift during data acquisition of only 1/3 part in 10^9 or 0.1 Hz doubles the observed line width to 0.2 Hz.

Achieving and maintaining field homogeneity around the sample is perhaps the most important and, at times, most frustrating experimental aspect of high field nmr. Small electromagnets called shimming coils are used to bend and shape the static magnetic field in the vicinity of the sample. When correctly tuned to optimize the local field homogeneity, the sharpest possible Lorentzian lineshapes in the frequency domain spectrum are obtained. One method of optimizing the shim settings is to maximize the deuterium lock signal intensity by adjusting the current in the individual shims. Alternatively, the FID or the lineshape for a strong resonance from the sample can be monitored as the shims are adjusted. There are two sets of adjustable shims. The vertical field gradients, which are aligned along the static field, B_0, are referred to as spinning or Z shims because these are set while the sample tube is spinning at 0–20 Hz around the z axis. These strongly affect the lineshape and linewidth of the observed signals. Typically, there are five orders of Z shims (Z, Z^2, Z^3, Z^4, Z^5) and all are interactive during the adjustment process. The horizontal field gradients, or nonspinning shims, are generally corrected to the third or fourth order with combinations of X, Y, and Z gradients. Typical gradients are X, Y, XZ, YZ, XY, X^2-Y^2, XZ^2, and YZ^2. Correct setting of these shims is most important in minimizing the satellite images of each signal called spinning sidebands; however, the higher order nonspinning shims also affect the lineshape and linewidth. These shim settings also are interactive. The initial shimming of a new instrument is a difficult process. Once reasonable settings have been made for each probe, however, the values are stored in a file on the acquisition computer. Usually, only small adjustments of Z, Z^2, and Z^3 need thereafter to be made for each sample (1,6).

The nmr probe is used to transmit and receive rf energy to and from the sample. Each manufacturer supplies specifications defining the achievable performance for each of their specific probes. Probe performance may be characterized in terms of the sensitivity and lineshape. Sensitivity is measured in terms of the signal-to-noise ratio for a single-pulse experiment on a specified sample. Linewidth is measured in several ways but the simplest involves a comparison of the full linewidth at 50% of maximum intensity. Probe sizes are defined in terms of the diameter of the sample tube that they accommodate and range, from 2.5 to 20 mm or larger. Probes are limited by the bore of the magnet in which they will be installed. Large probe diameters permit large sample volumes and are used for such insensitive nuclei as natural abundance ^{15}N or for samples that are poorly soluble. Small diameter probes are preferred when sample quantity is the limiting factor. Typically, 5-mm probes are used for routine

work as these have better lineshape specifications and shorter 90° pulse widths than the larger diameter probes. Variations in probe design and capabilities are numerous and are specific to particular types of analyses. Most probes contain one coil tuned to the deuterium lock frequency and two or more tunable coils. In broadband probes one of these coils can be tuned to one of the high frequency-range nuclei, such as ^{1}H, ^{3}H, or ^{19}F (see Table 1), whereas the other coil or coils each can be tuned to one of the other nuclei. Specifically tuned probes working at a single frequency or dual probes such as the H^1/C_{13} probe are also in common use. In general, the broadband or tunable probes are less sensitive but more versatile than the specifically tuned probe. Specialized probes are also required for solid-state measurements (7) and for gas-phase (8) studies.

Precisely controllable rf pulse generation is another essential component of the spectrometer. A short, high power radio frequency pulse, referred to as the B_1 field, is used to simultaneously excite all nuclei at the Larmor frequencies. The B_1 field should ideally be uniform throughout the sample region and be on the order of 10 μs or less for the 90° pulse. The width, in Hertz, of the irradiated spectral window is equal to the reciprocal of the 360° pulse duration. This can be used to determine the limitations of the sweep width (SW) irradiated. For example, with a 90° hard pulse of 5 μs, one can observe a 50-kHz window; a soft pulse of 50 ms irradiates a 5-Hz window. The primary requirements for rf transmitters are high power, fast switching, sharp pulses, variable power output, and accurate control of the phase.

The analogue-to-digital converter (ADC) samples the fluctuating voltage produced in the coils of the probe at regular time intervals, storing each value as a binary encoded integer. The rate at which the ADC must sample the voltage is defined by the Nyquist theorem, which states that the sampling rate must be greater than or equal to twice the signal frequency. The maximum speed of the digitizer determines the maximum observable spectral width; the number of bits used in storing each data point and the number of bits in each computer word determine the dynamic range of intensities that can be observed.

Quadrature detection is employed in nmr spectrometers to distinguish between positive and negative frequencies. This capability allows placement of the reference frequency in the center of the spectrum, thus reducing the required operating frequency of the ADC by a factor of two while increasing the sensitivity. In quad detection, two phase-sensitive detectors, 90° out of phase with one another, collect the time-domain spectrum as two independently digitized spectra. Fourier transformation of the resulting set of complex numbers are used to determine the relative positions and signs of the signals with respect to the reference frequency.

A computer-controlled bandpass filter system controls the size of the acquired spectral window. Typically, this is set to about 120% of the desired sweep width. Only frequencies within these limits are allowed to reach the ADC. Those frequencies outside the limits would only contribute to the noise in the final spectrum. The need for this system is dictated by the nonselective nature of the excitation rf pulse.

Modern nmr spectrometers are almost completely controlled by one or more computers (see COMPUTER TECHNOLOGY). Criteria for a computer system should include speed, compatibility with other systems, and the availability of large

amounts of rapidly accessible storage. The size of data arrays used in routine one-dimensional (1-D) nmr experiments is relatively small; however, when using 2-D or higher nmr experiments, the size is determined by the product of the number of points in each dimension and can become quite large, resulting in lengthy processing times. Most systems built up through the late 1980s contained integral computer systems that often contained vendor-specific memory structures. The trend as of the mid-1990s, however, is to employ standard personal computers or work stations made by computer companies. All of the principal systems now have separate software for acquisition and processing of spectra. By carrying out these functions on physically separate computers, ie, off-line processing, spectrometer use is not interrupted by lengthy processing steps. Software for off-line processing which can accept data from several different spectrometers is also available from third-party sources.

3.2. Electron Spin Resonance. Instrumentation for esr differs from nmr instrumentation principally as a consequence of the larger gyromagnetic ratio in this experiment. As a result, the external field is typically 0.35 T (3.5 kG). At this field strength the frequency associated with an unpaired electron is about 9.5 GHz (*X*-band). Systems operating at frequencies up to 34 GHz (*Q*-band) are also available. Fourier transform is becoming commonplace, but CW instruments also are widely used. Microwave radiation at a fixed frequency is produced by a Klystron valve at power levels ranging from less than 0.1 μW to several hundred mW and transmitted to the sample via rigid waveguides rather than the coaxial wire. The waveguide terminates in a reflection resonance cavity controlled by a microwave bridge. The function of this cavity is to focus the energy on the sample (see MICROWAVE TECHNOLOGY). In comparing systems, reference is made to the *Q* factor, ie, the ratio of the energy stored in the cavity to the energy lost in a cycle. *Q* factors of 5000–7000 are common. Esr signals typically become stronger at lower temperatures, and variable temperature systems capable of approaching liquid helium temperatures are available. Data are plotted in most applications as the first derivative spectrum. This presentation is more sensitive to changes in hyperfine structure than the absorption mode. Many esr spectrometers are also equipped to connect the electron nuclear double resonance (endor) experiment (9), which requires that the instruments supply rf at both the electron and nuclear frequencies.

Pulsed ft mode esr instruments have appeared beginning in the mid-1980s. These collect digitized time-domain spectra which may be processed into the frequency domain as are nmr data. Pulse durations are much shorter than in nmr with typical 90° times of 8–20 ns.

4. Health and Safety Factors

Safety considerations for magnetic resonance (mr) experiments have received little attention except for the problems associated with the use of electronic devices such as pacemakers in the magnetic field. However, in a 1990 study of reproductive health involving more than 1900 women working in clinical mr facilities in the United States no substantial differences were reported between the group of women directly involved with mr equipment (280 individuals) and other working

women (894 individuals) (10). Conclusions are restricted to exposure to the static external field.

5. The Nuclei of Nuclear Magnetic Resonance

Although nmr can be applied to many different nuclei, the overwhelming interest, especially for the organic chemist, continues to lie with ^{1}H and ^{13}C nmr. The hydrogen experiment is simpler because ^{1}H has a natural abundance of more than 99%, a large magnetogyric ratio, and a spin of 1/2. A three-stage model is commonly used to describe nmr experiments. Stages involve preparation, evolution, and detection periods.

5.1. Proton nmr. In the simplest experiment, the sample and a small amount of a reference compound such as tetramethylsilane [75-76-3] (TMS), $C_4H_{12}Si$, are placed in a tube, usually of 5-mm diameter. Typical samples may be a neat liquid or a solution containing as little solute as 0.01 mg/cm^3. The tube is positioned so that the sample lies in the coil. The spins are prepared by the application of a 90° rf pulse moving magnetization into the *xy* plane. In this experiment there is no evolution period, and detection commences as soon as the spins have been prepared. During detection the current in the detector coil is measured and digitized at regular time intervals and the results stored in a computer file. This cycle is one transient. After waiting for a suitable delay so that magnetic equilibration can occur, the entire cycle can be repeated. The results of the second experiment can be added to the first. After a suitable number of pulses have been acquired, the time-domain spectrum is transformed into a frequency-domain spectrum and phased so that the base line of the spectrum is flat and the peaks all fall on the same (positive) side of the base line. Information obtainable from this spectrum includes chemical shifts, coupling constants, and integrated peak areas.

Each hydrogen atom in a unique chemical environment is shielded differently from the external field and has a slightly different resonance frequency. The chemical shift in ppm, δ, is defined as

$$\delta = 10^6(\omega - \omega_{\mathrm{ref}})/\omega_0$$

where ω is the resonance frequency ofthe signal, ω_{ref} the frequency for a standard reference material, eg, the hydrogen in TMS in the case of ^{1}H. See Table 1 for reference materials for other nuclei. The Larmor frequency of the nucleus at the spectrometer's field is ω_0. The advantage of expressing shifts in ppm is that the scale is independent of the value of B_0. The value of the chemical shift can be correlated to the electronic environment of the nucleus, and extensive tables of chemical shift correlations are available in many sources (11). More precise databases specific to particular classes of compounds are also available in many instances.

The relative number of equivalent nuclei associated with each chemical shift is obtained from the integrated spectrum by normalizing the areas so that the area corresponding to the smallest peak in the spectrum is defined as 1. This relation may not be exactly correct in ft experiments where signals

may be affected by significant differences in relaxation times for nuclei in different environments.

When inequivalent nuclei are closely connected through covalent bonds, typically three or fewer, then the spin state of the proximate nuclei split the observed signal into multiple peaks through a process known as spin–spin coupling. In general, coupling of n equivalent nuclei of spin I gives rise to $2nI + 1$ lines where the intensity ratios follow the coefficients of a binomial expansion. The coupling pattern can be extremely useful in determining the chemical structure of an unknown compound. These patterns may become highly complex, however, when a nuclei couples to two or more inequivalent nuclei. In ethanol, for example, the methyl proton signal is a triplet having intensities in the ratio 1:2:1, the methylene proton signal is a quartet having intensity ratios 1:3:3:1, and, because of rapid exchange, the hydroxyl proton is a singlet. The triplet, for example, arises from the fact that the methylene protons, which are three bonds away, may have spins of either $+1/2$ or $-1/2$. This leads to four different combinations of spins. Two of these are degenerate because each has one proton at $+1/2$ and one proton at $-1/2$. The result is that the methyl protons are in three slightly different environments depending on the spins of the adjacent methylene group, and one of these states is twice as probable as either of the other two.

A second aspect of coupling is the separation between the lines in the multiplet. This spacing is equal between all lines in the multiplet if only a single coupling is involved. The strength of the coupling, ie, the coupling constant, J, is measured in Hz and is independent of B_0. An important consequence is that with increasing field strength, coupling patterns become more isolated from one another and thus easier to identify and interpret. Increasing the magnitude of B_0 simplifies spectral interpretation by isolating couplings from one another as shown in the similated spectra in Figure 4.

The magnitude of a coupling constant decreases as the number of intervening bonds between the coupled nuclei increases and typically three bonds, or ${}^3J$, is the detectable limit. The ${}^3J$ case is of particular interest because the magnitude of these constants is dependent on the conformation angle defined by the three bonds (12). The use of equations and theoretical approaches to the calculation of coupling constants has been reviewed (13). In general, the value of ${}^3J$ is maximum when coupled species are trans to one another. Within particular classes of compounds trigonometric functions of the torsion angle such as the Karplus equation may be used to predict the angle from the magnitude of the ${}^3J$.

The values of the time constants T_1 and T_2 are important in understanding both internal and overall motional behavior of the sample molecule. T_1 values are measured by the inversion recovery pulse sequence:

$$180^\circ - \tau - 90^\circ - \text{FID}$$

where 180° and 90° are rf pulses, and the preparation and detection steps, separated by a variable delay, τ, the evolution time. For each chemical shift the peak amplitude is measured as a function of τ and the value of T_1 is calculated from the following relation:

$$A_\tau = A[1 - 2\exp(-\tau/T_1)]$$

This process can be repeated thousands of times until adequate signal-to-noise is obtained providing that an initial recycling delay is inserted prior to the first pulse allowing restoration of magnetic equilibrium at the temperature of the experiment. This last delay should be 5–10 times longer than the longest T_1 which can be detected. The value of T_2 can be estimated from shapes of peaks in the absorption spectrum or measured exactly by the Carr-Purcell-Meiboom-Gill (CPMG) method (2). If these peaks are narrow, approaching the instrumentally limited linewidth, then $T_2 > T_1$, which is the case when the sample molecules are engaged in rapid tumbling such that $o_0\tau_c < 1$. As lines become broader, ie, T_2 becomes shorter, its value can be estimated from the following relation:

$$\Delta\overline{\omega}_{1/2} = (1/\pi)T_2^*$$

where the left-hand side representsthe actual measured line width and the asterisk T^*_2 indicates that this is an apparent T_2 which includes effects arising from inhomogeneity of the field. Very short T_2 values map into large, rigid molecular structures. Details of these measurements may be found in the general references (1,2) and in more specialized works (14).

The addition of paramagnetic species, such as the metal ions Cu^{2+}, Mn^{2+}, or Cr^{3+}, can have dramatic effects on both the observed spectrum and the relaxation behavior of a molecule. The added ion reduces nuclear relaxation times, T_1 and T_2, permitting more rapid data collection. In addition, faster relaxation rates minimize NOE effects in the spectra, which can be useful in obtaining quantitative ^{13}C intensity data. The most widely used reagent for this purpose is chromium acetylacetonate [13681-82-8], $Cr(C_5H_7O_2)_3$, known as $Cr(acac)_3$. Practically speaking, the use of such reagents requires care, because at high concentrations they may increase relaxation times and absorb strongly on the walls of the nmr tube. The use of these agents is particularly beneficial in achieving separations of peaks when working at lower field strengths. The line-broadening effect of these ions increases with the square of B_0; separation in chemical shift increases linearly with B_0 (15).

Lanthanide ions are used as contact shift reagents (2). The binding of these to specific sites in a molecule causes large changes in the ^1H chemical shifts that become progressively smaller as the distance between the ion and the proton increase. Although originally thought to proceed by the same mechanism as the paramagnetic chemical shift reagents, some contact shift reagents do not show the same external field dependence behavior. Some of these ions do not inhibit the measurement of NOE effects (16).

NOE difference spectroscopy is used to identify short, throughspace $^1H-^1H$ interactions and measure these interactions to an upper limit of about 0.45 nm. The experiment uses a selective pulse to irradiate a single frequency during the preparation delay. This transfers magnetization through space to nearby nuclei. A 90° pulse is then applied and the data collected. The experiment requires the acquisition of two or more separate spectra for the same sample. One is a control spectrum where the selective pulse is applied to the open part of the spectrum, and the others, in turn, select individual protons. After transformation, a difference spectrum is computed by subtracting the control from each of the

subspectra. The resulting spectra show NOE enhancements, either positive or negative, which measure the interaction between the irradiated signal and nearby hydrogen atoms. The magnitude of these effects is inversely proportional to the sixth power of the internuclear separation and can be used to estimate those distances.

Homonuclear decoupling, or spin decoupling, is a technique that simplifies the J coupling patterns of a spectrum (17). The pulse sequence uses two rf signals, ie, the normal hard 90° pulse irradiating the entire spectrum and a selective rf signal which saturates a particular spin. The selective pulse rapidly flips the energy states of the irradiated nucleus so that other coupled nuclei can only see the average orientation, and are therefore no longer coupled. This simplification of the J-coupling permits the identification of coupled spin systems and is particularly useful for determining coupling constants in a complex spin network. By sufficiently irradiating each multiplet in the spectrum sequentially the complete connectivity of the molecule can be determined. The two-dimensional (2-D) $^1H-^1H$ correlated spectroscopy (COSY) experiment yields the same information at a glance and is the preferred technique for direct determination of coupled spins.

The ID homonuclear Hartmann-Hahn (HOHAHA) experiment is an excellent way to determine complete coupled spin networks (18). The following pulse sequence is used:

$$\text{selective}\,90^\circ - 1/(2J) - \text{spin lock}$$

The selective 90° pulse is appliedto an isolated spin, thus aligning it along the y-axis; the $1/(2J)$ delay, where J is the coupling constant, allows the signal to rotate to the $-y$-axis. Then a spin-lock sequence is applied which maintains this orientation so that the spins no longer rotate about the z-axis, ie, no chemical shift differences exist. This allows the mixing or propagation of spins through the ^1H coupling network where directly and indirectly coupled spins can be observed. The spin-lock or mixing time can be varied to give subspectra with varying amounts of propagation. The longer the mixing time, the farther out from the source the spins propagate. This experiment can be used to make assignments of complex overlapped regions of a spectrum. A ^1H-edited spectrum is observed where the only observed spin network is the one which was selectively irradiated. The 1-D version has some advantages over the 2-D version of this experiment. By varying the spin-lock time from short to long periods, those spins which are 2, 3, 4, or even 5 positions removed from the source signal can be identified. However, in the 2-D experiment all signals are present, complicating the identification of propagation pathways.

The most common method of acquiring high resolution spectra of samples which are solids at the experiment temperature is solution nmr. If the nucleus under investigation is also found in the solvent, then the concentration of that nucleus in the solvent is usually far higher than in the sample, eg, pure water is 110 M in hydrogen. Such high concentrations can create severe dynamic range problems for detection of the sample. The historical method of solving this problem is to change the isotopic form of the solvent, for example by using deuterated solvents such as D_2O or $CDCl_3$. Alternatively, several techniques for

solvent suppression are possible. If the solvent signal is a single sharp line, eg, for pure water, the simplest method is selective saturation of the solvent resonance by continuous irradiation. Differences in relaxation times may also be employed because ^{1}H and ^{13}C often have longer relaxation times in small solvent molecules than in the sample species. In the water eliminated Fourier transform (WEFT) (2) water suppression sequence, for example, an initial 180° pulse is followed by a delay, a 90° pulse, and acquisition of the FID. The value of the delay is set so as to minimize the height of the water peak. During this period, the magnetization of the sample is restored to $+z$ so that the net effect on the sample is the same as a 90° pulse. Other techniques for water suppression include spin echo techniques (19), Dante (2) sequences, and most recently gradient field methods such as WATERGATE (20).

5.2. Carbon-13 NMR. Carbon-13 [14762-74-4], ^{13}C, nmr (1,2,11) has been available routinely since the invention of the pulsed ft/nmr spectrometer in the early 1970s. The difficulties of studying carbon by nmr methods is that the most abundant isotope, ^{12}C, has a spin, I, of 0, and thus cannot be observed by nmr. However, ^{13}C has $I = 1/2$ and spin properties similar to ^{1}H. The natural abundance of ^{13}C is only 1.1% of the total carbon; the magnetogyric ratio of ^{13}C is 0.25 that of ^{1}H. Together, these effects make the ^{13}C nucleus ca 1/5700 times as sensitive as ^{1}H. The interpretation of ^{13}C experiments involves measurements of chemical shifts, integrations, and J-coupling information; however, these last two are harder to determine accurately and are less important to identification of connectivity than in ^{1}H nmr.

Observation of homonuclear $^{13}C-^{13}C$ coupling is very unlikely because of the low probability for bonding between two ^{13}C atoms. In addition, ^{13}C coupling is not easily observable in the ^{1}H nmr spectrum because of ^{13}C's low natural abundance. The J_{CC} couplings, which may range from 35–175 Hz, can be used to determine $^{13}C-^{13}C$ connectivity using experiments such as the 1-D INADEQUATE technique, which filters out the single-quantum signals, ie, those signals arising from uncoupled nuclei. Heteronuclear coupling from ^{1}H to ^{13}C is easily observed: $^{1}J_{CH}$ values are large, ranging from 110–330 Hz, typical $^{2}J_{CH}$ and $^{3}J_{CH}$ values are between 0 and 12 Hz. The observation of a completely coupled ^{13}C spectrum would have so many overlapping multiplets that it would be difficult to interpret. To simplify this problem, the energy levels of the ^{1}H nuclei are saturated by irradiation using a broadband decoupling frequency eliminating coupling to the ^{13}C atoms. This process, which yields a proton-decoupled ^{13}C spectrum, is the standard method for ^{13}C nmr. Decoupling has two effects: all multiplets are collapsed into singlets, one for each nonequivalent ^{13}C atom; and the transfer of NOE from the excited ^{1}H to the ^{13}C signals enhances some peaks by up to 200%. The relative intensities of individual peaks in a ^{13}C spectrum are also affected by differences in T_1 values of the atoms. Normally, the relative intensities of ^{13}C nmr signals diminish in the order of CH_3, CH_2, CH, C.

Quantitation of ^{13}C nmr intensities employs inverse gated decoupling experiments, where the ^{1}H decoupling rf is turned off during a preparation period and then turned on during the acquisition period, thereby eliminating NOE influences on the decoupled spectrum. Ideally, elimination of relaxation-time effects requires that the preparation period should be at least five times longer than the largest T_1 expected. Thus acquisition times for these experiments are

quite long. When only qualitative information is sought, buildup of the NOE during the preparation time is actually desirable, because NOE increases the SNR in each transient. In addition the preparation time period can be decreased to 1–3 times that of T_1. Care must be employed to avoid saturation of quaternary ^{13}atoms.

Spectral editing refers to any method which alters the appearance of the spectrum so that specific structural features become readily identifiable. This may include elimination of signals from solvent molecules, and changes in disposition of peaks in a ^{13}C spectrum with respect to the baseline as a function of the number of directly coupled ^{1}H nuclei. Polarization transfer, or population transfer, as it is sometimes called, involves shifting characteristics, eg, energy and spin state, of the abundant spin magnetization to ^{13}C or some other nucleus and therefore is an important experimental approach to spectral editing. Two examples of spectral editing techniques are the INEPT and DEPT experiments. Simultaneous transfer of polarization from all ^{1}H nuclei to all of X nuclei can be accomplished using the insensitive nuclei enhanced by polarization transfer (INEPT) method (2). A serious drawback of INEPT is the fact that triplets and other multiplets are not immediately recognizable, because intensities are distorted. The distortionless enhancement by polarization transfer (DEPT) method eliminates this drawback and can directly distinguish among methyl, methylene, methine, and quaternary carbons (2). The technique uses polarization transfer from sensitive nuclei such as ^{1}H, ^{19}F, or ^{31}P to insensitive nuclei, ie, ^{13}C, ^{29}Si, or ^{15}N (see Table 1). One final advantage of polarization transfer-based methods is an increase in sensitivity of γ_S/γ_I where the subscripts refer to the sensitive and insensitive nuclei, respectively.

5.3. Other Nuclei. Although most nmr experiments continue to involve ^{1}H, ^{13}C, or both, many other nuclei may also be utilized. Several factors, including the value of I for the nucleus, the magnitude of the quadrupolar moment, the natural abundance and magnetogyric ratio of the isotope, or the possibility of preparing enriched samples, need to be considered. The product of the isotopic parameters can be compared to the corresponding value for ^{13}C, providing a measure of relative sensitivity or receptivity. Table 1 summarizes these factors for a number of isotopes. More complete information may be found in the literature (21,22).

For nuclei where $I > 1/2$, such as deuterium, ^{2}H, there are two important differences from spin $I = 1/2$ systems. First, different coupling patterns occur when $I \geq 1$, and secondly, significant line broadening is a consequence of medium-to-large quadrupolar moments. The simplest and most commonly occurring example of the coupling effects is evident when a proton-decoupled ^{13}C spectrum is obtained for a compound dissolved in $CDCl_3$. Because ^{2}D has $I = 1$, and there are $2nI + 1$ spin states, the carbon spectrum shows a 1:1:1 triplet at 77.0 ppm arising from deuterium–carbon coupling in the solvent. The nuclear electric quadrupolar moment, Q, which may be positive or negative, is usually reported in units of barn, where 1 barn1barn $= 10^{-28}$m^2. In general, values of $|Q|$ range between 6.4×10^{-32}m^2 (^{6}Li) and 3×10^{-28} (^{181}Ta). When present, the quadrupolar process is the most efficient of the relaxation processes available to a nucleus. Hence its rate controls the line width of the signal.

The fluorine-19 [14762-94-8], ^{19}F, nucleus has a sensitivity second only to that of ^{1}H. Moreover, the frequency is similar enough to ^{1}H's that often the signal can be detected by tuning the proton channel of a probe to the ^{19}F frequency. In addition to the usual chemical shift and coupling experiments, ^{19}F nmr of fluorinated ligands is widely applicable in kinetic studies of enzyme–substrate interactions (23) (see KINETIC MEASUREMENTS). The success of this approach depends on the larger enzyme-induced changes in ^{19}F chemical shifts, as compared to ^{1}H chemical shifts in the parent compound. Such protein-induced changes are typically 9–15 ppm in a downfield direction. The danger in interpreting such studies is that the replacement of hydrogen by fluorine may also have significant effects on the structure and stability of a complex. A second problem for fluorine is the large chemical shift anisotropy (CSA). The effect of this property on the magnetic-field dependence of both T_1 and T_2 increases the natural linewidth with increasing B_0.

Phosphorus-31 [7723-14-0], ^{31}P, also is readily accessible for nmr because of its spin of 1/2, 100% natural abundance, magnetogyric ratio of 10.8, 600-ppm chemical shift window, and moderate relaxation times. Early ^{31}P studies were done in CW mode (24,25). The availability of ft instrumentation led to improved sensitivity such that analysis of millimolar solutions in standard 5-mm tubes has become routine. Technically, the primary difficulty lies in achieving satisfactory digital resolution using this large chemical shift window. Both the large chemical shift literature and theoretical approaches to the ^{31}P chemical shift are discussed elsewhere (26). The occurrence of phosphorus in cell membrane phospholipids and in nucleotides has led to its use as a reporter on structure and dynamics in enzyme complexes, cell membranes, and nucleic acids as well as organophosphorous compounds (27). In nucleic acid studies the ^{31}P chemical shift is considered to report on both local conformation and sequence. The assignments of specific resonances to individual nucleotides usually involves HETCOR-type studies of $^{31}P-^{1}H$ correlations similar to $^{13}C-^{1}H$ studies of multidimensional nmr (28). Among the more unique applications of ^{31}P is its applicability to the study of *de novo* metabolic pathways for the synthesis of phosphatidylcholine and other membrane phospholipids (29,30). In these studies the samples are living perfused cells or organs, or intact organisms, and the probes are specifically designed for the application.

Although the natural abundance of nitrogen-15 [14390-96-6], ^{15}N, leads to lower sensitivity than for carbon-13, this nucleus has attracted considerable interest in the area of polypeptide and protein structure determination. Uniform enrichment of ^{15}N is achieved by growing protein synthesizing cells in media where $^{15}NH_4OH$ is the only nitrogen source. $^{15}N-^{1}H$ reverse shift correlation via double quantum coherence permits the complete assignment of all ^{15}N resonances. Because there is one such nitrogen in the main chain for each amino acid, complete assignments, ^{1}H scalar coupling, hydrogen exchange experiments, and NOE studies taken together can provide a detailed picture of the protein conformation and the kinetics of protein folding. An example of this approach is available in the literature (31). Details of the enrichment experiments and of the application of two-dimensional techniques such as COSY, TOCSY, and NOE experiments to the products have been reviewed (32). Because of the large number of resolvable distance-sensitive data which may be obtained by

these experiments, the reliability of conformational studies by nmr for small and intermediate-sized proteins are likely to be dramatically improved.

The nmr relaxation behavior and chemical shift effects of metal ions in solution may provide considerable insight into metal ion-containing systems. The presence of such ions may induce significant changes in the ^{1}H spectrum and, if the ion is sitebound, the magnitude of such effects decreases sharply with increasing distance between the ion and the proton. Secondly the chemical shifts and line profiles of the ion itself are both sensitive to the binding state and to the distribution of ions between bound and free states providing a probe for the kinetics of binding. Finally, when the ion is paramagnetic, quadrupolar relaxation mechanisms become the predominant mechanism for loss of magnetization (33).

6. Multidimensional NMR

The first two-dimensional (2-D) nmr experiment was proposed in 1971 at an nmr conference (1). Multidimensional nmr underwent explosive growth in the 1980s and early 1990s and impinges on all aspects of modern nmr. In a typical 2-D experiment, a set of related FIDs are acquired using the same basic pulse sequence while systematically varying the evolution time. The experiment is illustrated schematically in Figure 5 which shows the steps in obtaining a correlated spectroscopy (COSY) spectrum. In the acquisition process, several FIDs are acquired sequentially under identical preparation and acquisition conditions, but at varying evolution times, t_1, resulting in a family of FIDs. By convention, the time axis is t_2 as shown in Figure 5**b**. Fourier transformation of any single row leads to a frequency-domain spectrum along the F_2 axis. If all rows are processed using identical phasing constants and a vertical line is drawn through the spectra at any point f_2 on the F_2 axis, then the intensity of the signal at that point oscillates as a function of the evolution time (Fig. 5**c**). A Fourier transform of this time-dependent signal leads to a second frequency-domain, F_1, spectrum. The resulting two-dimensional matrix contains maxima and minima corresponding to coupled interactions between the two frequency domains (Fig. 5**d**). In a homonuclear experiment, the F_1 and F_2 domains are identical whereas this is not so in a heteronuclear experiment. The nature of the interaction creating these peaks and valleys depends on the particular pulse sequence employed. In general, the interactions may arise from J-coupling, through space interactions, or from polarization transfer. Finally, each pulse sequence (Fig. 5**a**) could be extended using one or more evolution times and additional pulses leading to third or higher dimensions in the spectrum.

The first example of a multinuclear experiment is the homonuclear proton COSY experiment (1,2,34). A typical ^{1}H COSY spectrum is that of Figure 5**d** where the conventional one-dimensional ^{1}H spectrum is evident along both the F_2 and F_1 axes, as well as along the diagonal. Starting from any cross-peak at position (f_1, f_2), lines parallel to F_1 and F_2 can be extended to the diagonal. Ideally, the pattern is symmetric across the diagonal and this leads to the formation of a box where the two symmetry-related cross-peaks are corners, and two J-coupled peaks on the diagonal are the other corners. Although the

COSY spectrum can be generated in several ways, the simplest pulse sequence is $90^\circ - t_1 - 90^* - t_2 - \text{FID}$ where t_1 is the variable evolution time and t_2 is the acquisition time. Interpretation of COSY spectra, in simple cases, is straightforward and unambiguous in the identification of coupled proton spin systems. For strongly coupled systems, ie, where $[f_2 - f_1(\text{Hz})] < 10$, cross-peaks may occur indistinguishably close to the diagonal. Suppression of the true diagonal peaks by double-quantum filtering (DQF-COSY) may resolve such problems. Finally, quantitative measurements of the magnitude of the coupling constants is possible using the *Z*-COSY modification. These experiments are restricted to systems of abundant spins such as ^{1}H, ^{11}B, and ^{31}P, which have reasonably narrow linewidths.

A 2-D total correlated spectroscopy (TOCSY), or HOHAHA experiment (2) resembles a homonuclear COSY. The pulse sequence differs from the COSY in that the 90° pulse after the evolution time is replaced by a mixing time. This mixing time is used to lock the spins onto the *y*-axis which allows isotropic mixing of the spin systems. As in the 1-D HOHAHA experiment, choosing a short mixing time yields data very similar to a COSY, ie, directly coupled spins produce cross-peaks, whereas the use of long mixing times includes the complete spin system. An example of a 2-D-TOCSY having a mixing time of 120 ms is given in Figure 6**a**. As for the 1-D HOHAHA several 2-D TOCSYs can be run at different mixing times to determine the number of bonds over which the spins have propagated. The advantage of the 2-D experiment over the 1-D version is that all the information is acquired in one experiment. However, if only a small number of spin networks need to be determined, then the experiment of choice is the 1-D HOHAHA.

TOCSY data are acquired in the phase-sensitive mode using quadrature detection, and all the data phases are positive. This increases the SNR for the matrix, and the time required for the experiment is short because very little, if any, phase cycling is necessary. In some cases a single scan per FID suffices, and the data can be acquired in approximately 10 min.

Heteronuclear chemical shift-correlated spectroscopy, commonly called H-X COSY or HETCOR has, as the name implies, different F_1 and F_2 frequencies. The experiment uses polarization transfer from the ^{1}H nuclei to the ^{13}C or X nuclei which increases the SNR. Additionally, the repetition rate can be set to 1–3 T_1 of the ^{1}H rather than the longer ^{13}C. Using the standard ^{1}H–^{13}C COSY, the amplitude of the ^{13}C signals are modulated by the *J*-coupled frequencies of the ^{1}H nuclei in the evolution time. The projection of the F_2 axis is an edited ^{13}C spectrum where only those carbons having attached protons are observed. The projection of the F_1 axis is an edited ^{1}H spectrum where only protons attached to ^{13}C are observed. Figure 6**b** shows a standard HETCOR. The existence of a cross-peak indicates a direct correlation of the ^{1}H peak to the ^{13}C peaks. To identify these peaks, simply draw a line from the ^{13}C signal on the F_2 axis to the cross-peak and then a second line parallel to the F_1 axis identifies the directly coupled proton. The sample requirements are similar to those of a standard ^{13}C experiment. Interpretation of the ^{13}C spectrum is straightforward if the ^{1}H spectrum has been assigned and this is an excellent way to determine diastereotopic protons because these produce two ^{1}H signals for one ^{13}C signal.

An alternative way of acquiring the data is to observe the ^{1}H signal. These experiments are referred to as reverse- or inverse-detected experiments, in particular the inverse HETCOR experiment is referred to as a heteronuclear multiple quantum coherence (HMQC) spectrum. The amplitude of the ^{1}H nuclei is modulated by the coupled frequencies of the ^{13}C nuclei in the evolution time. The principal difficulty with this experiment is that the ^{13}C nuclei must be decoupled from the ^{1}H spectrum. Techniques used to do this are called GARP and WALTZ sequences. The information is the same as that of the standard HETCOR except that the F_1 and F_2 axes have been switched. The obvious advantage to this experiment is the significant increase in sensitivity that occurs by observing ^{1}H rather than ^{13}C.

Another important inverse experiment is the heteronuclear multiple bond correlation (HMBC) spectrum; its ^{13}C observed counterpart experiment is the COLOC (35), which suffers from lack of sensitivity. The HMBC detects long-range coupling from protons to carbon atoms separated by two to three bonds, while suppressing the directly attached proton–carbon correlations. This is useful when making assignments of isolated spin groups such as methoxy, carbonyl, and quaternary carbon groups, because there is typically at least one proton set that is within the two to three-bonds range for any given carbon in an organic molecule. The projection of either an HMBC or an HMQC spectrum contains ^{13}C chemical shift information, which can be useful when working with samples that are too dilute to permit the acquisition of a standard ^{13}C spectrum.

The 2-D incredible natural abundance double-quantum transfer experiment (INADEQUATE) was developed in the late 1980s (35,36). This experiment, as the name implies, is not applicable to most real samples because of the large quantity of sample required. The signals that are being observed are the ^{13}C satellites arising from the ^{13}C–^{13}C coupling. The natural abundance of ^{13}C is 1.1% of the total carbon, and therefore the likelihood of a covalent bond between two ^{13}C atoms is 1:10,000. Also, the normal single-quantum ^{13}C signals must be suppressed by phase cycling. Hence the experiment has low sensitivity and experiment times are long. The 2-D INADEQUATE yields a great deal of information, however. The F_2 axis contains the standard ^{13}C spectrum and F_1 is the double-quantum frequency of $\nu_1 + \nu_2$, where ν_1 and ν_2 are the frequencies of the coupled spins, measured in Hz from the center band frequency. When the experiment is set up correctly, its interpretation is straightforward, and the molecular carbon skeleton can be deduced. Highly concentrated solutions, as well as the addition of a relaxation reagent such as $Cr(acac)_3$ to shorten the preparation delay, are helpful.

The 2-D nuclear Overhauser effect spectroscopy (2-D-NOESY) experiment resembles the ^{1}H–^{1}H COSY; however, the cross-peaks arise from chemical exchange or from the NOE effects, not J-coupling. The experiment yields data similar to a series of transient NOE difference experiments for all chemical shifts. The pulse sequence is $90^\circ - t_1 - 90^\circ - t_m - 90^\circ$, where t_1 is the evolution time, t_m is the mixing time, and t_2 is the detection time. The second 90° pulse restores the frequency-labeled transverse magnetization back to the z-axis. During the mixing time, t_m, the magnetization on the z-axis is allowed to mix and a 90° pulse is applied to read the information. The data are collected in the phase-sensitive mode. Positive NOEs are phased up, whereas the diagonal

negative NOEs and chemical exchange cross-peaks are phased down. COSY-type peaks may also appear. Typically, a series of 2-D-NOESY spectra, each having a different mixing time, are collected and compared to the corresponding COSY spectrum to determine which signals arise from J-coupling, which from chemical exchange, or which from NOEs. NOE buildup curves are used to determine internuclear distance constraints (2). The intensity of the effect varies with r_{ij}^{-6}, and only interactions with $r_{ij} < 0.5$nm are detectable. The NOESY experiment is particularly applicable to large molecules such as proteins, nucleic acid, polysaccharides, or synthetic polymers because on the nmr time scale, macromolecules tumble relatively slowly, producing large ($\leq 50\%$) negative NOEs suitable for quantification. Because of rapid tumbling, small molecules can have positive, negative, or no NOE even if the distances are within the proper magnitude. The rotating frame nuclear Overhauser effect spectroscopy (ROESY) (2,5) experiment is best suited for small- to intermediate-sized molecules. The ROESY replaces the evolution time with a spin-lock field so that the effective precession frequency is very small. This makes even the largest molecules appear to be tumbling rapidly and makes all NOE signals positive.

Given the possibility of making complete assignments of all chemical shifts in molecules as large as small proteins and the availability of both distance- and angle-dependent nmr parameters, attempts are being made to determine the three-dimensional structure of molecules from nmr, and nmr-restrained molecular modeling (qv) methods are being developed as an alternative to x-ray diffraction (36). One such approach is distance geometry (37), which uses the short, throughspace contacts identified in NOESY experiments to formulate a set of mathematical restraint equations which tend to force the selected interatomic distances to assume suitably short values. Using a sufficient number of such interactions for each residue in a polymer chain, it should be possible to correctly identify probable structures from the nmr data alone. Other computer programs elastically restrain torsion angles to values estimated from ^3J-coupling constants. A second and somewhat different approach involves using the nmr restraints to augment the molecular mechanics forcefield in a molecular dynamics calculation (38). In this approach the basic forcefield contains terms describing contributions to the potential energy arising from bond stretching, bond-angle deformation, torsional interactions, van der Waals interactions, and electrostatic interactions. The additional nmr term contains equations designed to satisfy coupling and NOE data for the molecule. Finally, a kinetic energy term is also included where the total kinetic energy at a temperature, T, is $3N(kT/2)$ where $3N$ is the number of degrees of freedom for a system of N atoms, and kT is the usual Boltzmann energy term. The entire system is then allowed to fluctuate in terms of atomic positions and velocities by solving the Newtonian equations of motion at very closely spaced intervals in time. All of the molecular dynamics algorithms including CHARMm, Discover, GROMOS, and AMBER permit the calculation of such restrained dynamics. Both the distance geometry approach and, to a lesser degree, the dynamics approach can have problems with structures becoming locked in local minima. A second problem is that whereas a crystal structure typically involves a unique set of atomic coordinates describing the position of each atom, the structure of a

molecule in solution may involve several coexisting conformers contributing to a time- and space-averaged structure.

There are many instrumental considerations in multidimensional spectroscopy. These are important in defining the appropriate digital resolution in F_1 and F_2. Unlike 1-D nmr, the data size in 2-D experiments can become quite large very rapidly if the wrong parameters are used. For instance, using a 32-bit integer word size, a 2k $\times$ 2k data set occupies at least 16 Mb and even more if phase-sensitive data is being acquired. The best way to determine the minimum number of data points required in F_2 is to run a routine 1-D spectrum and determine the minimum acceptable Hz per point from it. Because F_1 resolution is a function of the number of evolution time increments, ie, the number of separate FIDs which must be stored, the resolution in the F_1 dimension is much lower than in the F_2 dimension. The minimum necessary F_1 digitization can also be determined from the number of Hz per points needed to resolve signals in the 1-D spectrum. As for 1-D nmr, zero-filling and optimal window functions can be used to improve the apparent resolution in the 2-D matrix.

Time constraints are an important factor in selecting nmr experiments. There are four parameters that affect the amount of instrument time required for an experiment. A preparation delay of 1–3 times T_1 should be used. Too short a delay results in artifacts showing up in the 2-D spectrum whereas too long a delay wastes instrument time. The number of evolution times can be adjusted. This affects the F_1 resolution. The acquisition time or number of data points in t_2 can be adjusted. This affects resolution in F_2. Finally, the number of scans per FID can be altered. This determines the SNR for the 2-D matrix. In general, a lower SNR is acceptable for 2-D than for 1-D studies.

Window functions for 2-D nmr are necessary because of the poor digital resolution in both dimensions. The short acquisition time required by the small number of data points in the F_2 domain and the limited number of evolution times for F_1 domain means that the data is being truncated. The software provided by any of the manufacturers provides several different window functions including exponential decays, shifted sinebell, shifted sinebell squared, Gaussian, and trapezoidal functions. The best function to use depends on the type of information sought. Often it is best to process the data using several different functions to determine the best choice for that particular data set.

7. High Resolution Solid-State NMR

The ability to acquire high resolution nmr data from solid phases is critical to many applications where, for example, test samples are insoluble, exploration of a nascent structure is desired, or samples are cross-linked (39,40). However, as seen by comparing Figures 7**a** and 7**d,** the use of liquid-phase nmr experiments using solid samples leads to broad lines having little discernible structural detail. Three principal problems in obtaining nmrs of solids are chemical shift anisotropy (CSA), a high degree of dipolar interactions, and very long (10^2–10^3 s) T_1 values typical of rigid molecules. The first two characteristics have origins in the comparative absence of motional averaging in solid samples. The Hamiltonians describing both the chemical shift and dipolar interactions are actually

tensors, 3×3 matrices, where the interaction is a function of the orientation of the molecular axis system with respect to the laboratory axis system. Motional averaging in solution reduces both to scalar quantities which are actually the trace, ie, the average of the diagonal components of the tensor, and all off-diagonal components average to 0 (2).

As originally proposed in 1962, magic-angle spinning (MAS), where the sample is rapidly rotated about an axis inclined to B_0 by 54.74°, the magic angle, produces considerable line sharpening. This reduction in linewidth is a consequence of the off-diagonal elements in both the CSA and dipolar interaction tensors leading to terms of the form $3\cos_2\theta - 1$ where θ is the angle between B_0 average orientation of dipoles in the sample. At the magic angle this term is equal to 0. The reduction in signal away from the central line is incomplete because it is rarely possible to spin the sample fast enough. Typical spinning speeds in MAS probes are 4–7 kHz although the newest probes can achieve rates of 27 kHz.

A further reduction in the dipolar interaction term is achieved by dipolar decoupling. In the simplest case this is accomplished by replacing the usual liquid-phase decoupler with a much higher power decoupler, $\geq$100 W. Using both of these techniques together results in a considerable sharpening of the lines, as shown in Figure 7**c**. The intensity, however, is quite weak and, owing to the long T_1 values, the preparation delay is extremely long. Hartman-Hahn matching for cross-polarization (CP), ie, polarization transfer, minimizes the time required for repolarization of the carbon atoms. In this technique a 90° pulse and spin-locking of the ^{1}H magnetization into the transverse, *xy,* plane is followed by simultaneous rf irradiation such that the Hartman-Hahn condition is met for a time period referred to as a mixing time or contact time, t_c, which is usually about 1 ms.

$$\gamma_H B_{1H} = \gamma_C B_{1C}$$

Because both spins are in the transverse plane and transition energy levels are matched, energy can be transferred from the protons to the ^{13}C nuclei. In this manner the rate of ^{13}C repolarization is controlled by T_{1H} rather than by T_{1C}. Because the protons can interchange energy by spin-diffusion only a single-proton T_1 exists and its value is usually on the order of 1 s. As a result the preparation delay can be reduced from 10^3 s to about 5 s increasing the number of transients, which can be acquired by two or more orders of magnitude.

One difficulty with this method is that the optimal mixing time for different carbon environments is not the same; as a result, the integrated intensities are even less quantitative than in liquid-phase ^{13}C nmr. A compromise value is selected by varying the mixing time systematically and looking for a value that provides an adequate signal for all resonances. A second difficulty is that the benefit derived from CP decreases with increasing proton–X nucleus distance so that it really only affects atoms having covalently bound hydrogen. Thus, quaternary carbon atoms and other X nuclei such as ^{31}P are insensitive to CP. The increase in intensities seen in Figure 7**b** as compared to 7**c** results from the use of CP. One additional feature apparent in Figure 7**b** is the existence of a number of additional lines not found in the liquid spectrum (Fig. 7**a**). These

lines may originate from any of several sources. Because elimination of CSA is incomplete, the CSA is sampled by sidebands separated from each central resonance by a multiple of the spinning rate. These sidebands may be useful, as they sample the complete CSA, or they may be eliminated using sideband suppression modifications to the pulse sequence. A second source of additional lines results from different phases within the sample, ie, crystalline and amorphous phases, having somewhat different chemical shifts and line profiles for each resonance. Even in crystalline samples, if two different crystalline forms co-exist or if the crystal structure contains chemically identical molecules which are not related by symmetry, multiple peaks may occur.

One final technical improvement in solid-state nmr is the use of combined rotational and multiple pulse spectroscopy (CRAMPS) (2), a technique which also requires a special probe and permits the acquisition of high resolution ^{1}H and X nucleus nmr from solids. The combination of these methods permits adapting most of the 1-D and 2-D experiments previously described for liquids to the solid phase.

Applications of solid-state nmr include measuring degrees of crystallinity, estimates of domain sizes and compatibility in mixed systems from relaxation time studies in the rotating frame, preferred orientation in liquid crystalline domains, as well as the opportunity to characterize samples for which suitable solvents are not available. This method is a primary tool in the study of high polymers, zeolites (see MOLECULAR SIEVES), and other insoluble materials.

8. Electron Spin Resonance

Esr is also a powerful technique both alone or in combination with nmr in the endor method (9). Precise measurements of the hyperfine couplings and lineshape lead to detailed information concerning the structure and conformation of molecules containing unpaired electrons. It is perhaps the most powerful tool for studying structure in free-radical containing species and as such plays an important role in understanding reaction mechanisms. A second area of current importance is the study of radiation-induced changes in chemicals. The attachment of spin labels to different parts of a molecule also provides a method of probing local structure.

BIBLIOGRAPHY

"Analytical Methods" in *ECT* 3rd ed., Vol. 2, pp. 586–683, by E. Lifshin and E. A. Williams, General Electric Co.

CITED PUBLICATIONS

1. A. E. Derome, *Modern NMR Techniques for Chemical Research*, Pergamon Press, Oxford, U.K., 1987.

2. J. K. M. Sanders and B. K. Hunter, *Modern NMR Spectroscopy: A Guide for Chemists*, 2nd ed., Oxford University Press, Oxford, U.K., 1993.
3. L. Kevan and M. K. Bowman, eds., *Modern Pulsed and Continuous-Wave Electron Spin Resonance*, John Wiley & Sons, Inc., New York, 1990.
4. R. N. Bracewell, *The Fourier Transform and Its Applications*, 2nd rev. ed., McGraw-Hill Book Co., Inc., New York, 1986.
5. D. Neuhaus and M. P. Williamson, *The Nuclear Overhauser Effect in Structural and Conformational Analysis*, Verlag Chemie, New York, 1989.
6. W. W. Conover, in G. C. Levy, ed., *Topics in Carbon-13 NMR Spectroscopy*, Vol. **4**, John Wiley & Sons, Inc., New York, 1984, 38–51.
7. E. Fukushima and S. B. W. Roeder, *Experimental Pulse NMR: A Nuts and Bolts Approach*, Addison-Wesley Publishing Co., Inc., Reading, Mass., 1981.
8. C. J. Jameson, *Chem. Rev.* **91**, 1375–1395 (1991).
9. C. F. Poole, Jr. and H. A. Farach, eds., *Handbook of Electron Spin Resonance: Datasources, Computer Technology, Relaxation and ENDOR*, American Institute of Physics, New York, 1994.
10. E. Kanal, J. Gillen, J. A. Evans, D. A. Savitz, and F. G. Shellock, *Radiology* **187**, 395–399 (1993).
11. R. M. Silverstein, C. Bassler, and T. C. Morrill, *Spectrometric Identification of Organic Compounds*, John Wiley & Sons, Inc., New York, 1991.
12. M. Karplus, *J. Chem. Phys.* **30**, 11 (1959).
13. R. H. Contreras and J. C. Facelli, *Ann. Rep. NMR Spectrosc.* **27**, 256–356 (1993).
14. D. J. Craig and G. C. Levy, in G. C. Levy, ed., *Topics in* ^{13}C NMR Spectroscopy, Vol. **4**, John Wiley & Sons, Inc., New York, 1984, 239–275.
15. A. Carrington and A. D. McLachlan, *Introduction to Magnetic Resonance*, Harper and Row, New York, 1967, 221–229.
16. J. M. Bulsing, J. K. M. Sanders, and L. D. Hall, *J. Chem. Soc. Chem. Commun.*, 1201–1203 (1981).
17. R. A. Hoffman and S. Forsen, *Prog. N.M.R. Spectrosc.* **1**, 15–204 (1966).
18. D. G. Davis and A. Bax, *J. Am. Chem. Soc.* **107**, 7197–7198 (1985).
19. V. Sklenár and A. Bax, *J. Magn. Reson.* **75**, 378 (1987).
20. V. Saudek, M. Piotto, and V. Sklenár, *Bruker Report* **140**, 6–9 (1994).
21. P. Laszlo, *NMR of Newly Accessible Nuclei*, Vols. **1** and **2**, Academic Press, New York, 1979.
22. C. Brevard and P. Granger, *Handbook of High Resolution Multinuclear NMR*, John Wiley & Sons, Inc., New York, 1981.
23. J. T. Gerig, *Methods Enzymol.* **177B**, 3–23 (1989).
24. W. C. Dickenson, *Phys. Rev.* **81**, 717 (1951).
25. H. S. Gutowsky and D. W. McCall, *Phys. Rev.* **82**, 748 (1951).
26. D. G. Gorenstein, ed., *Phosphorus-31 NMR: Principals and Applications*, Academic Press, San Diego, Calif., 1994.
27. D. G. Gorenstein, *Methods Enzymol.* **177B**, 295–316 (1989).
28. C. R. Calladine, *J. Mol. Biol.* **161**, 343 (1982).
29. S. M. Cohen, *Methods Enzymol.* **177B**, 417–434 (1989).
30. P. F. Daly, R. C. Lyon, P. J. Faustino, and J. S. Cohen, *J. Biol. Chem.* **262**, 14875 (1987); J. S. Cohen, R. C. Lyon, and P. F. Daly, *Methods Enzymol.* **177**, 435–452 (1989).
31. P. Varley, A. M. Gronenborn, H. Christensen, P. T. Wingfeld, R. H. Pain, and G. M. Clore, *Science* **260**, 1110–1113 (1993) and Ref. 6 therein.
32. D. C. Muchmore, L. P. McIntosh, C. B. Russell, D. E. Anderson, and F. W. Dahlquist, *Methods Enzymol.* **2177B**, 43–73 (1989).
33. C. R. Sanders II and M.-D. Tsai, *Methods Enzymol.* **2177B**, 317–333 (1989).

34. A. Bax and R. Freeman, *J. Am. Chem. Soc.* **104**, 1099 (1981).
35. W. E. Hull, in W. R. Croasmun and R. M. K. Carlson, eds., *Two-Dimensional NMR Spectroscopy: Applications for Chemists and Biochemists*, VCH Publishers, New York, 1987.
36. A. Bax, *Ann. Rev. Biochem.* **58**, 223–256 (1989).
37. G. M. Crippen and T. F. Havel, *Distance Geometry and Molecular Conformation*, John Wiley & Sons, Inc., New York, 1988.
38. J. DeVlieg and W. F. van Gunsteren, *Methods Enzymol.* **202**, 268–300 (1991).
39. J. L. Koenig, *Spectroscopy of Polymers*, American Chemical Society, Washington, D.C., 1992, 197–256.
40. R. Komoroski, ed., *High Resolution NMR Spectroscopy of Synthetic Polymers in Bulk*, VCH Publishers, New York, 1986.

DAVID J. KIEMLE
WILLIAM T. WINTER
State University of New York, Syracuse

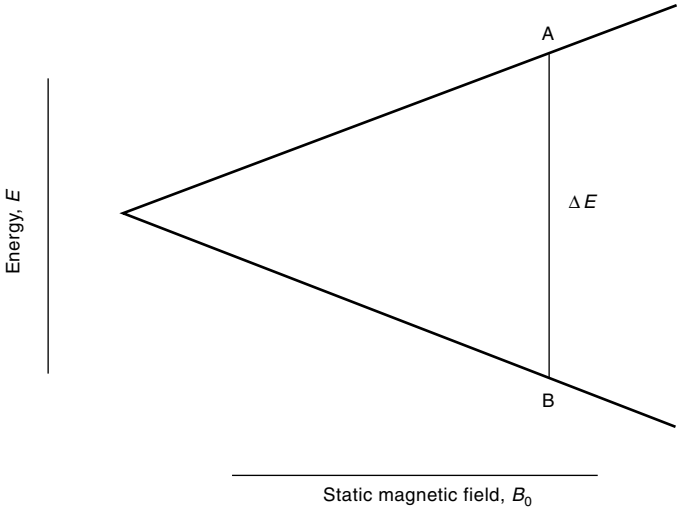

Fig. 1. Schematic representation of energy, E, vs external field strength, B_0, for a nucleus of spin, $I = 1/2$. A, spin $= -1/2$; B, spin $= 1/2$.

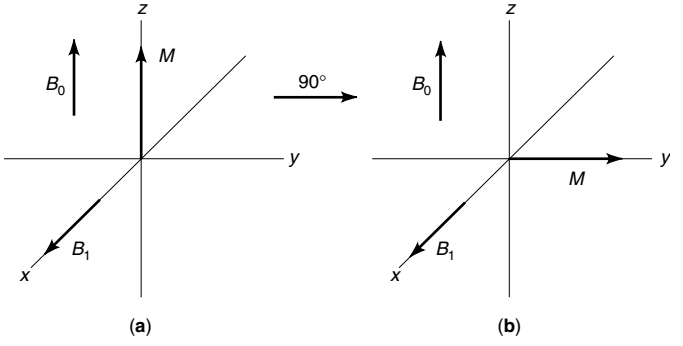

Fig. 2. Interaction of nucleus (electron) with static magnetic field, B_0, where the bulk magnetization, M, is (**a**) parallel to B_0 and to the z-axis, and (**b**), upon application of a 90° radio frequency pulse along x, M perpendicular to B_0 and to the z-axis. See text.

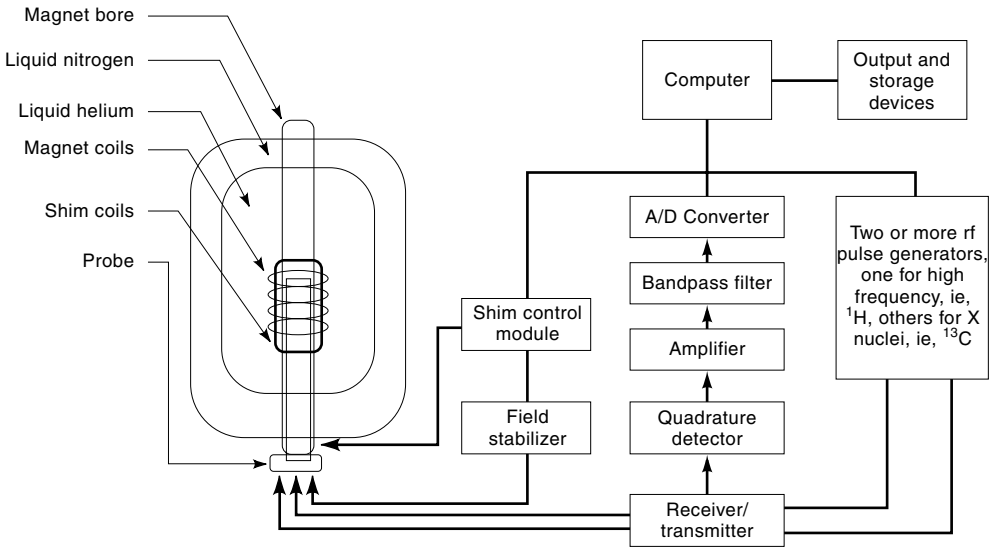

Fig. 3. A block diagram schematic representation of a Fourier transform nmr spectrometer, ie, a superconducting magnetic resonance system.

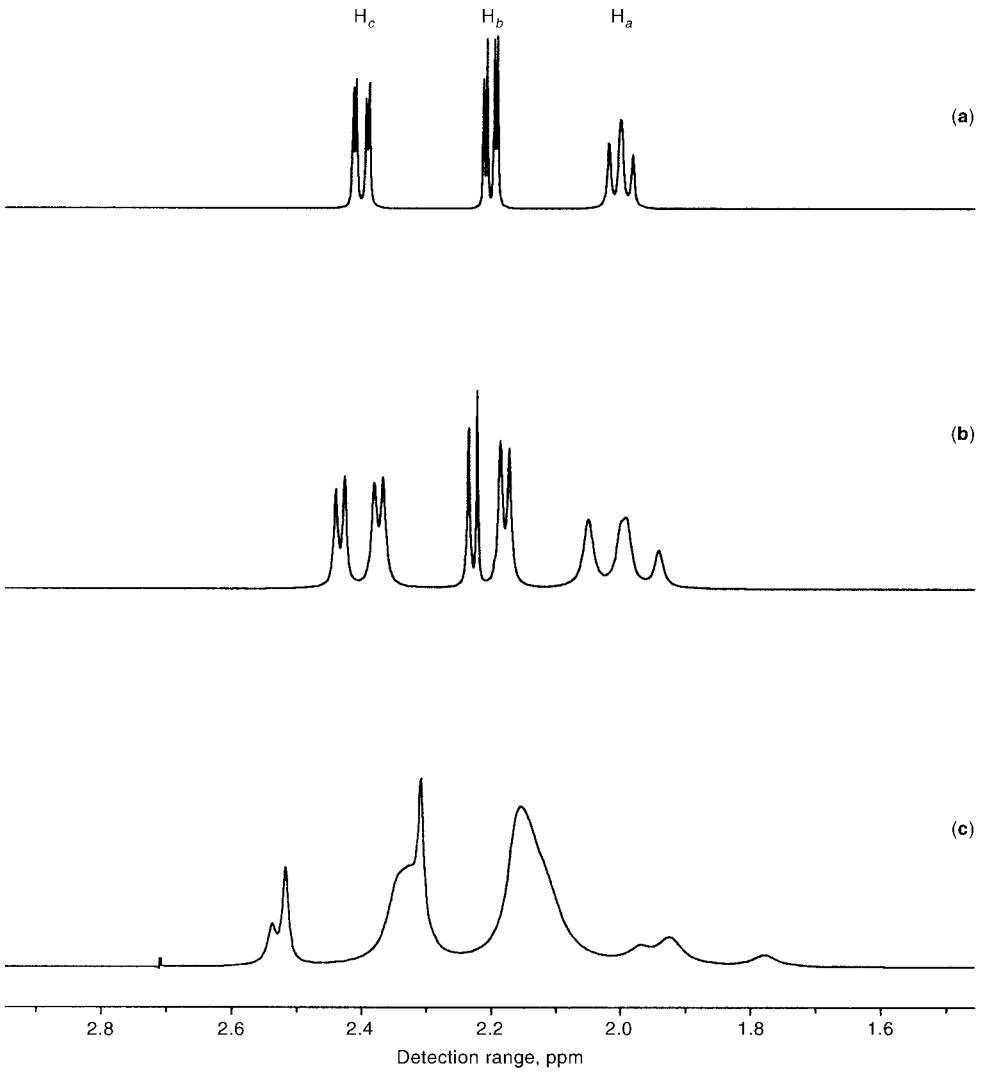

Fig. 4. Simulated ^{1}H nmr spectrum for a molecule having three interacting spin systems H_a, H_b, and H_c where $J_{ab} = 10\text{Hz}, J_{bc} = -3\text{Hz}$, and $J_{ac} = 12\text{Hz}$ at (**a**) 600 MHz, (**b**) 200 MHz, and (**c**) 60 MHz.

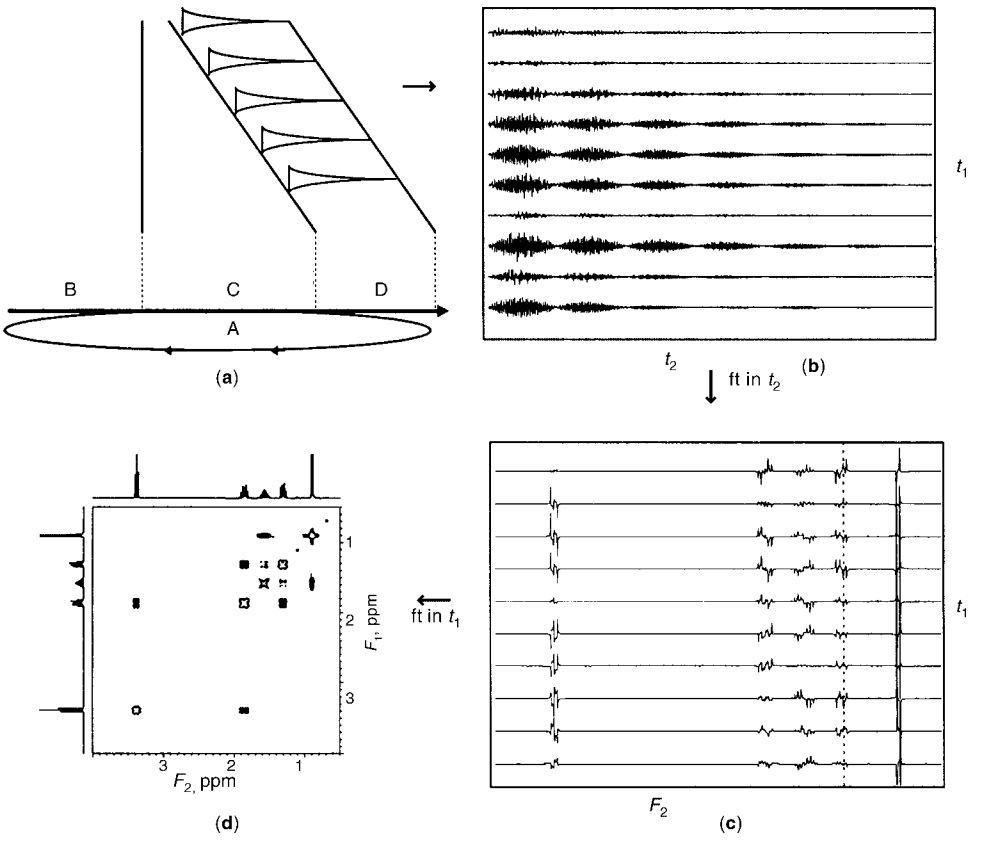

Fig. 5. A 2-D nmr experiment of 2-methyl-5-bromopentane [626-88-0], $C_6H_{13}Br$, where t_1 and t_2 correspond to evolution and acquisition time, respectively. (**a**) A set of pulsing experiments differing in evolution times leading to (**b**) a set of related FIDs to which a Fourier transform in t_2 is applied. Each FID leads to (**c**) a set of spectra; and a second Fourier transform along t_1 results in (**d**) the COSY spectrum. In (**a**), A indicates the progression of time through B, preparation, C, evolution and mixing, and D, acquisition. See text.

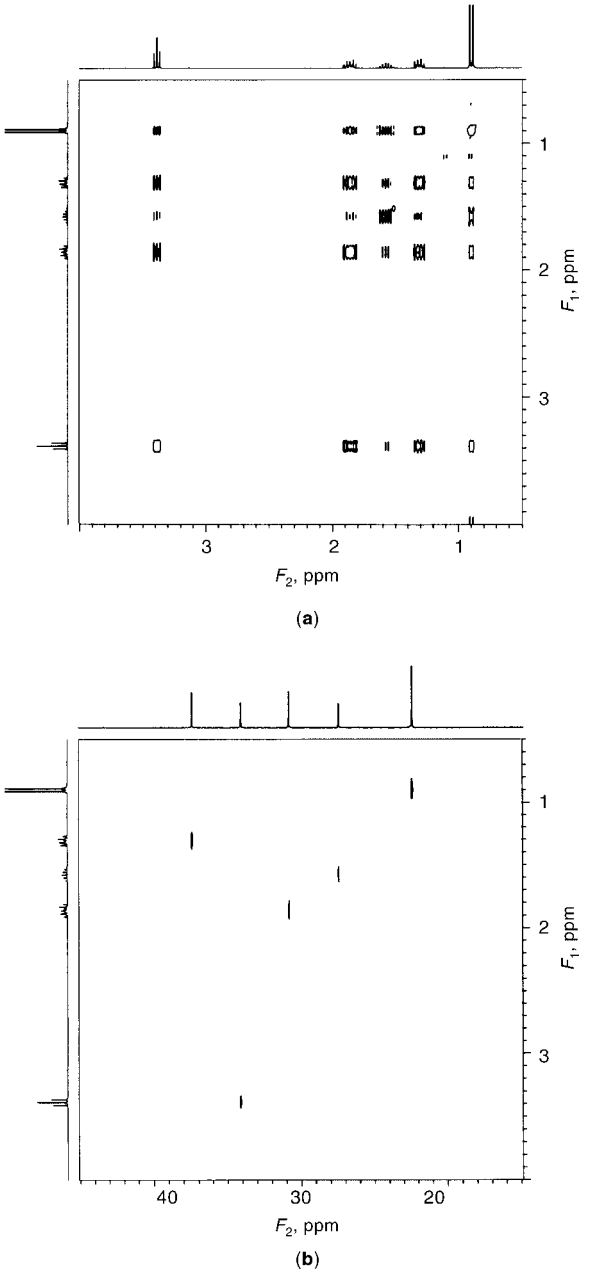

Fig. 6. Spectra of 2-methyl-5-bromopentane acquired using a Bruker 300AMX spectrometer: (**a**) TOCSY using a 5-mm $^{13}C-^{1}H$ dual probe and (**b**) HMQC using a 5-mm inverse detection broadband probe.

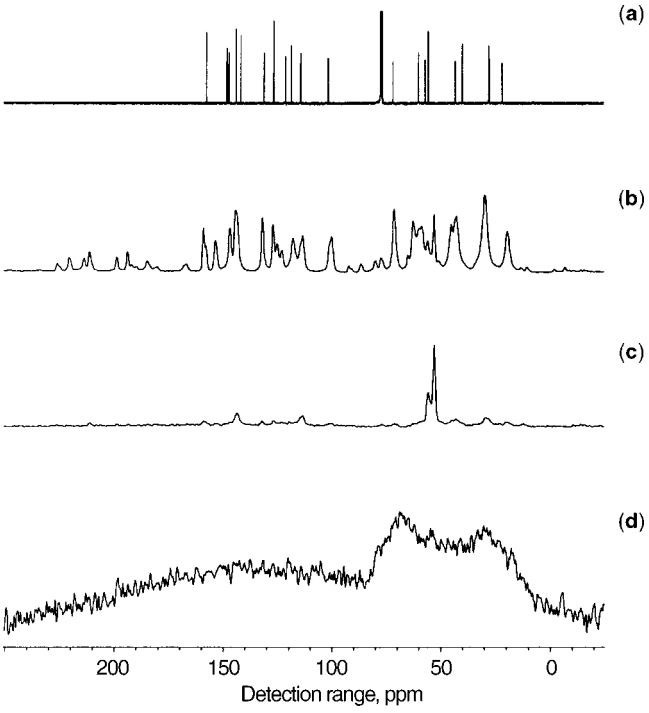

Fig. 7. Nmr spectra of quinine [103-95-0], $C_{20}H_{24}N_2O_2$, acquired on a Bruker 300AMX spectrometer using a Bruker broadband CP/MAS probe. (**a**) Proton-decoupled ^{13}C spectrum of quinine in $CDCl_3$; (**b**) the corresponding spectrum of solid quinine under CP/MAS conditions using high power dipolar decoupling; (**c**) solid-state spectrum using only MAS and dipolar decoupling, but without cross-polarization; and (**d**) solid quinine run using the conditions of (**a**).

Table 1. **Nmr Parameters for Less Commonly Used Nuclei $10^{-28}m^2$**

Isotope	Spin, I	Receptivity ratio[a]	Reference compound	Detection range, ppm	ν at 7.05 T,[b] MHz[c]	Q,[d]
^{2}D	1	0.008	$Si(CD_3)_4$	10 to 0	46.5	0.00027
^{6}Li	1	3.58	$LiCl_2/D_2O$	2 to −10	44.15	−0.0006
^{11}B	3/2	754.00	$BF_3/(C_2H_5)O$	65 to −130	96.21	0.0355
^{14}N	1	5.69	NH_3 (l)[e]	900 to 0	21.68	0.016
^{15}N	1/2	0.022	NH_3 (l)[e]	900 to 0	30.41	
^{17}O	5/2	0.061	H_2O	1700 to −50	40.67	−0.026
^{19}F	1/2	4730.00	$CFCl_3$	−276 to −280	282.23	
^{23}Na	3/2	525.00	1*M* $NaCl/H_2O$	10 to −65	79.35	0.12
^{25}Mg	5/2	1.54	$MgCl_2/H_2O$	50 to −25	18.36	0.22
^{27}Al	5/2	117.00	$Al(NO_3)_3$	240 to −240	79.70	0.149
^{29}Si	1/2	2.09	$Si(CH_3)_4$	80 to −380	59.60	
^{31}P	1/2	377.00	85% H_3PO_4	270 to −480	181.04	
^{35}Cl	3/2	20.2	NaCl in H_2O	1200 to −100	29.39	−0.08
^{39}K	3/2	3.69	KCl in H_2O	10 to −25	14.00	0.055
^{43}Ca	7/2	0.53	$CaCl_2$ in H_2O	40 to −40	20.19	−0.05
^{47}Ti	5/2	0.864	$(TiF_6)^{2-}$	1700 to 0	16.92	0.29
^{71}Ga	3/2	319.00	$Ga(H_2O)_6^{3+}$	650 to −800	72.00	0.178
^{75}As	3/2	143.00	$KAsF_6$	370 to −300	51.37	0.3
^{77}Se	1/2	2.98	$Se(CH_3)_2$	2000 to −800	57.21	
^{81}Br	3/2	277.00	$NaBr/H_2O$	100 to −500	81.02	0.28
^{87}Rb	3/2	277.00	$RbCl/H_2O$	50 to −230	98.16	0.12
^{89}Y	1/2	0.668	$Y(ClO_4)_3$	20 to −140	14.70	
^{99}Ru	5/2	0.83	1*M* RuO_4/CCl_4	3000 to −3300	13.84	0.076
^{113}Cd	1/2	7.6	$Cd(ClO_4)_2/H_2O$	850 to −100	66.53	
^{117}Sn	1/2	19.5	$Sn(CH_3)_4$	500 to −2300	58.62	
^{127}I	5/2	530.00	NaI/H_2O	4000 to −500	60.03	−0.79
^{129}Xe	1/2	31.80	$XeOF_4$ neat	2000 to −5300	82.97	
^{139}La	7/2	336.00	$10^{-2}M$ $LaCl_3/H_2O$	310 to −20	42.38	0.21
^{195}Pt	1/2	19.1	Na_2PtCl_6	9000 to −4000	64.39	
^{199}Hg	1/2	11.8	$Pb(CH_3)_4$	11200 to −6000	62.57	

[a] The receptivity ratio is calculated by comparing the value of $a_x\gamma_x^3 I_x(I_x+1)$ to the corresponding value for ^{13}C, where a_x = abundance of x, γ_x = magnetic ratio, and I_x = spin$x$. See text.
[b] To convert T to G, multiply by 1.00×10^4.
[c] Corresponding to 300 MHz for ^{1}H.
[d] Q = electric quadrupolar moment.
[e] At 25°C.